An explosive mud volcano origin for the pitted cones in southern Utopia Planitia, Mars

Le WANG[1,2†], Jiannan ZHAO[3†], Jun HUANG[1,2*], Long XIAO[1,2]

1 School of Earth Sciences, China University of Geosciences, Wuhan 430074, China.

2 State Key Laboratory of Geological Processes and Mineral Resources, Wuhan 430074, China.

3 Key Laboratory of Geological Survey and Evaluation of Ministry of Education, China University of Geosciences, Wuhan 430074, China.

Corresponding author: Jun Huang, junhuang@cug.edu.cn

†The authors contribute equally.

Abstract

Pitted cones are cone-shaped structures, spanning from meters to kilometers in size, characterized by summit depressions. They are widely distributed on the surface of Mars with various origins, such as rootless cones, mud volcanoes, cinder or scoria cones, tuff rings or cones, pingos, and dirt cones. If the pitted cones identified in southern Utopia Planitia are mud volcanoes, as is speculated, they could be of particular interest due to the fact that mud volcanoes on Earth bring sediments from depth of meters to kilometers to the surface. In this study, we have investigated the pitted cones near Zhurong rover's landing site in southern Utopia Planitia, utilizing recent images and digital elevation models obtained from the High Resolution Imaging Camera instrument onboard China's Tianwen-1 orbiter. By leveraging the high-resolution images and digital elevation models, we have conducted a geometric measurement to distinguish the origin of pitted cones in the vicinity of the Zhurong rover. The morphological characteristics of these pitted cones indicate an explosive mud volcano origin. These explosive mud volcanoes could have formed by the violent eruption of subsurface overpressurized sediments generated from the combined effect of overburden pressure and anomalous high heat flow. The sediments forming the pitted cones in the northern plains could be the remnants of an ancient ocean. With future in-situ observations of these pitted cones, we hope to gain further insights into the sediments of the putative northern ocean, as well as the physical and chemical properties of the Martian subsurface during the formation of the pitted cones.

Keywords: pitted cones, mud volcanoes, Tianwen-1, Mars

1. Introduction

China's first Mars exploration mission Tianwen-1 entered the orbit of Mars on February 10, 2021, with the onboard Zhurong rover successfully landing on the surface of Mars in the southern Utopia Planitia (109.925 °E, 25.066 °N) on May 15, 2021 (Liu et al., 2022a). Various landforms have been identified in the Zhurong landing area, including pitted cones, polygonal troughs, ridges, mesas, and aeolian bedforms (Zhao et al., 2021). Among these landforms, pitted cones, cone-shaped structures with meter- to kilometer-scale basal diameters and summit depressions, stand as the most prominent landforms in the landing area of the Zhurong rover. Previous studies have shown that pitted cones with various morphologies and sizes are widely distributed in the northern lowlands (Figure 1), such as Utopia Planitia, Isidis Planitia, Elysium Planitia, Acidalia Planitia, Chryse Planitia, and Amazonis Planitia (Frey and Jarosewich, 1982; Fagents et al., 2002; Lanz and Saric, 2009; Lanz et al., 2010; Keszthelyi et al., 2010; Brož and Hauber, 2012; Brož and Hauber, 2013; Noguchi and Kurita, 2015; Komatsu et al., 2016; Brož et al., 2019; B. Wu et al., 2021; X. Wu et al., 2021; Ye et al., 2021) and in small basins of the southern highlands (Hemmi and Miyamoto, 2017), north of Olympus Mons Aureole (Hodges and Moore, 1994) and Kamativi crater (Keszthelyi et al., 2010). Several origins have been proposed for the pitted cones, including rootless cones and fumarolic cones (Fagents et al., 2002; Xiao and Wang, 2009; Noguchi and Kurita, 2015), scoria/cinder cones (Lanz et al., 2010; Brož and Hauber, 2012; Brož et al., 2017), tuff rings/cones (Brož and Hauber, 2013), dirt cones (Kargel et al., 1995; Guidat et al., 2015), pingos (Burr et al., 2009a; de Pablo and Komatsu, 2009) and mud volcanoes (Skinner and Tanaka, 2007; Oehler and Allen, 2010; Salvatore and Christensen, 2014; Orgel et al., 2019; Komatsu et al., 2016; Ye et al., 2021).

The study of martian pitted cones mainly involves examining their terrestrial analogs in conjunction with the regional geologic context. For example, pitted cones in the Tharsis area are proposed to be scoria/cinder cones based on evidence such as the basal lava flow-like feature and the volcanic geology of the area (Brož and Hauber, 2012). Pitted cones in the Nephentes-Amenthes region (southern Utopia Planitia boundary plain) are considered to be tuff rings/cones resulting from phreatomagmatic explosive eruptions (Brož and Hauber, 2013). The morphometric results indicate that these cones are similar to tuff rings/cones on Earth (Brož and Hauber, 2013). In addition to morphological measurement, the evidence of subsurface water ice and volcanic activity within or around the Nephentes-Amenthes region are also important arguments for the phreatomagmatic origin of the cones reported by Brož and Hauber (2013). For most of the pitted cones distributed along the margins of the northern plains, mud volcano is the prevalent origin (Oehler and Allen, 2010; Ivanov et al., 2014; Salvatore and Christensen, 2014; Ye et al., 2021). From a mineralogical perspective, the presence of minerals formed in the aqueous sedimentary environment can provide strong evidence for the origin of the mud volcano. Spectral data has identified hydrated minerals and nanophase ferric minerals on the summit pits, suggesting hydration alteration (Oehler and Allen, 2010; Komatsu et al., 2016; Dapremont and Wray, 2021). However, it is difficult to determine whether these minerals formed contemporaneously with the cones or through later alteration processes. Therefore, the interior samples of the pitted cones are required to determine their evolutionary history. The thermal inertia of most pitted cones is relatively low (Oehler and Allen, 2010; Salvatore and Christensen, 2014), indicating that the particle size of the materials is relatively fine. The identification of their orbital spectral characteristics is challenging (Komatsu et al., 2016) due to dust cover, making in-situ investigation necessary to determine composition and origin of the pitted cones. This study examines the morphology of pitted cones in the Zhurong landing region using high-resolution images obtained by the Tianwen-1 orbiter and discusses their likely origin of the pitted cones. We also propose possible future in-situ observations of the Zhurong rover on these pitted cones.

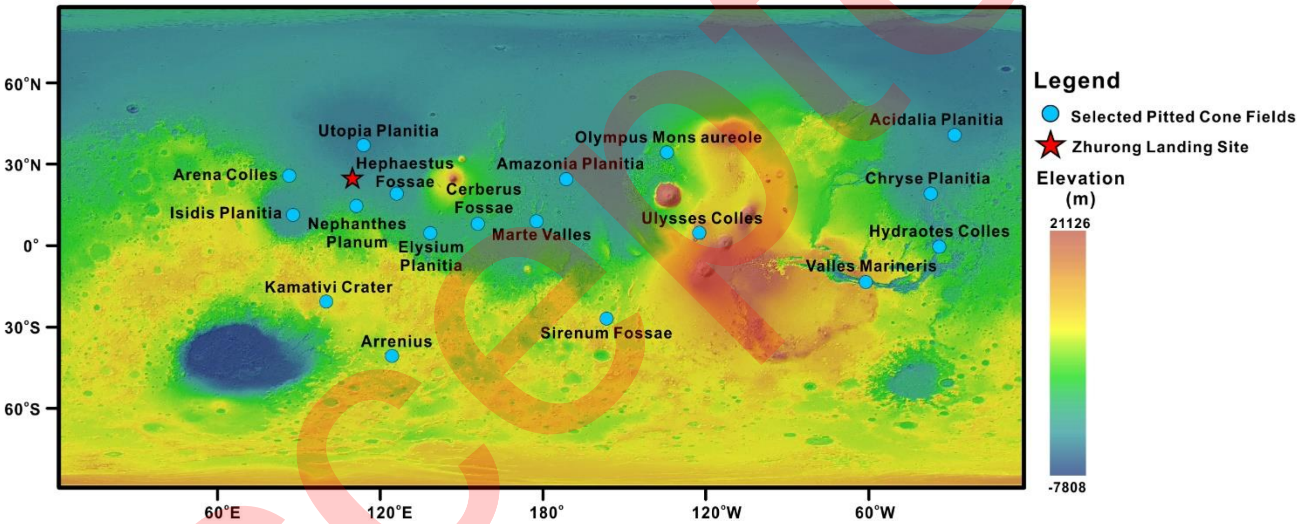

Figure 1 Selected pitted cone fields on Mars. The red star indicates the landing site of the Zhurong rover. The background is color-coded MOLA MEGDR (Smith et al., 2001) merged with a MOLA shaded relief map.

2. Geologic Setting

The study area is the landing region of Zhurong, within southern Utopia Planitia (Figure 1). This area is situated in the Vastitas Borealis Formation (VBF), which is interpreted as the remnants of an ancient ocean (e.g., Parker et al., 1989, 1993; Clifford and Parker, 2001; Ivanov and Head, 2001; Mouginot et al., 2012; Ivanov et al., 2014). The VBF, covering most area of northern lowlands, was formed by the deposition of outflow channel materials during the Late Hesperian to Early Amazonian period (Carr and Head, 2003; Tanaka et al., 2003; Mouginot et al., 2012). The presence of low dielectric constant materials and widely distributed rampart craters suggest the existence of subsurface ice in the VBF (Mouginis-Mark, 1987; Mouginot et al., 2012). Recent studies have reported layered subsurface and evidence of aqueous activities during Amazonian period in the Zhurong landing area (Liu et al., 2022b; Li et al., 2022), which further supports the presence of

https://engine.scichina.com/doi/10.1007/s11430-022-1119-1

sedimentary processed in the study area.

3. Data and Methods

High Resolution Imaging Camera (HiRIC) onboard the Tianwen-1 orbiter captured images with a spatial scale of 0.7 m pixel^{-1} (Yan et al., 2021; Zou et al., 2021). The digital elevation models (DEMs; 3.5 m pixel^{-1}) with an elevation error of about 1 m and a planar position error of 0.4 m (Yan et al., 2022) was produced using stereo HiRIC images (Meng et al., 2021; Liu et al., 2022a; Yan et al., 2022). Compared to the Context Camera data (CTX, ~6 m pixel^{-1}) (Malin et al., 2007), HiRIC has a higher resolution. Although the resolution of HiRIC is slightly lower than that of the High Resolution Imaging Science Experiment data (HiRISE ~25–30 cm pixel^{-1}) (McEwen et al., 2007), the HiRIC has a larger coverage area in the Zhurong landing region. Therefore, we utilized the high-resolution images and DEMs from HiRIC for detailed morphological measurement of the pitted cones.

In the morphological studies of pitted cones both on Earth and Mars, basal diameter (Wco), summit crater diameter (Wcr), height (Hco) (Figure 2a), and their ratios (e.g., Wcr/Wco, Hco/Wco, and Hco/Wcr), as well as the slopes (Figure 2a) are critical parameters to constrain the origin of the pitted cones (Wood, 1979; Pike, 1978; Brož and Hauber, 2013; Dapremont and Wray, 2021; Huang et al., 2022). To acquire these geometric parameters, we used the slope analysis tool of Quantum Geographic Information Systems (QGIS) to generate a slope map of the study region based on the HiRIC DEMs. We then extracted the pixels with slope values greater than 5 degrees, which allowed us to well define the base edges and summit craters of the pitted cones (Figure 2b). Subsequently, we used the circle construction tool of QGIS to make a vectorization of the base edges and summit craters (Figure 2b), enabling us to acquire the Wco and Wcr through the field calculator. By analyzing the HiRIC DEMs, we also determined the mean elevations of the base edges and summit craters, and the differences of the two elevations yielded Hco. Using the trigonometric relationship of Wco, Wcr, and Hco (equation (1)), we calculated the slope of the pitted cones. In this step, we excluded pitted cones with elongated plan-view shapes and significant erosion from the morphometric analysis, as their geometric parameters could not be accurately measured.

$$slope = \arctan\left(\frac{2Hco}{Wco - Wcr}\right) \quad (1)$$

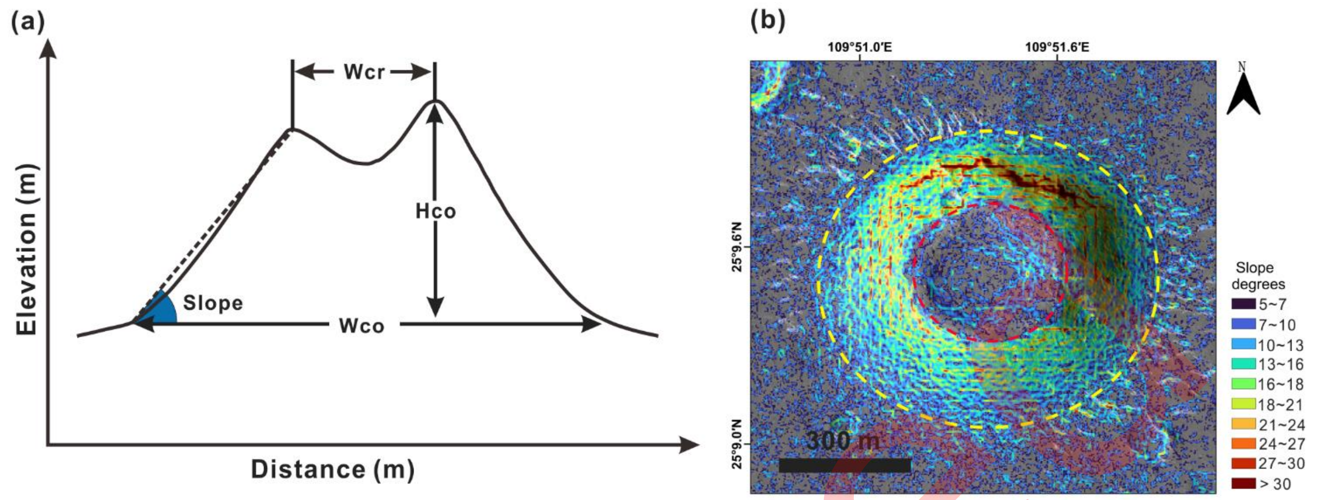

Figure 2 Measurement method of the pitted cones. (a) Parameters were measured for each pitted cone. Wco, Wcr, and Hco are basal diameter, summit crater diameter, and height, respectively. Note that height is an average value. (b). The slope map overlain on the HiRIC image (HX1_GRAS_HIRIC_DIM_0.7_0004_251515N1095850E _A), the yellow circle indicates the base edge and the red circle indicates the margin of the summit depression of the pitted cone.

4. Results

We identified 112 pitted cones in the study area (Figure 3a). The nearest cone (marked by a white triangle in Figure 3a) is ~14.5 km away from the Zhurong rover along its traveling direction (Figure 3b). After excluding the elongated and the intensely eroded pitted cones, 69 among the 112 pitted cones were used to measure the geometric parameters.

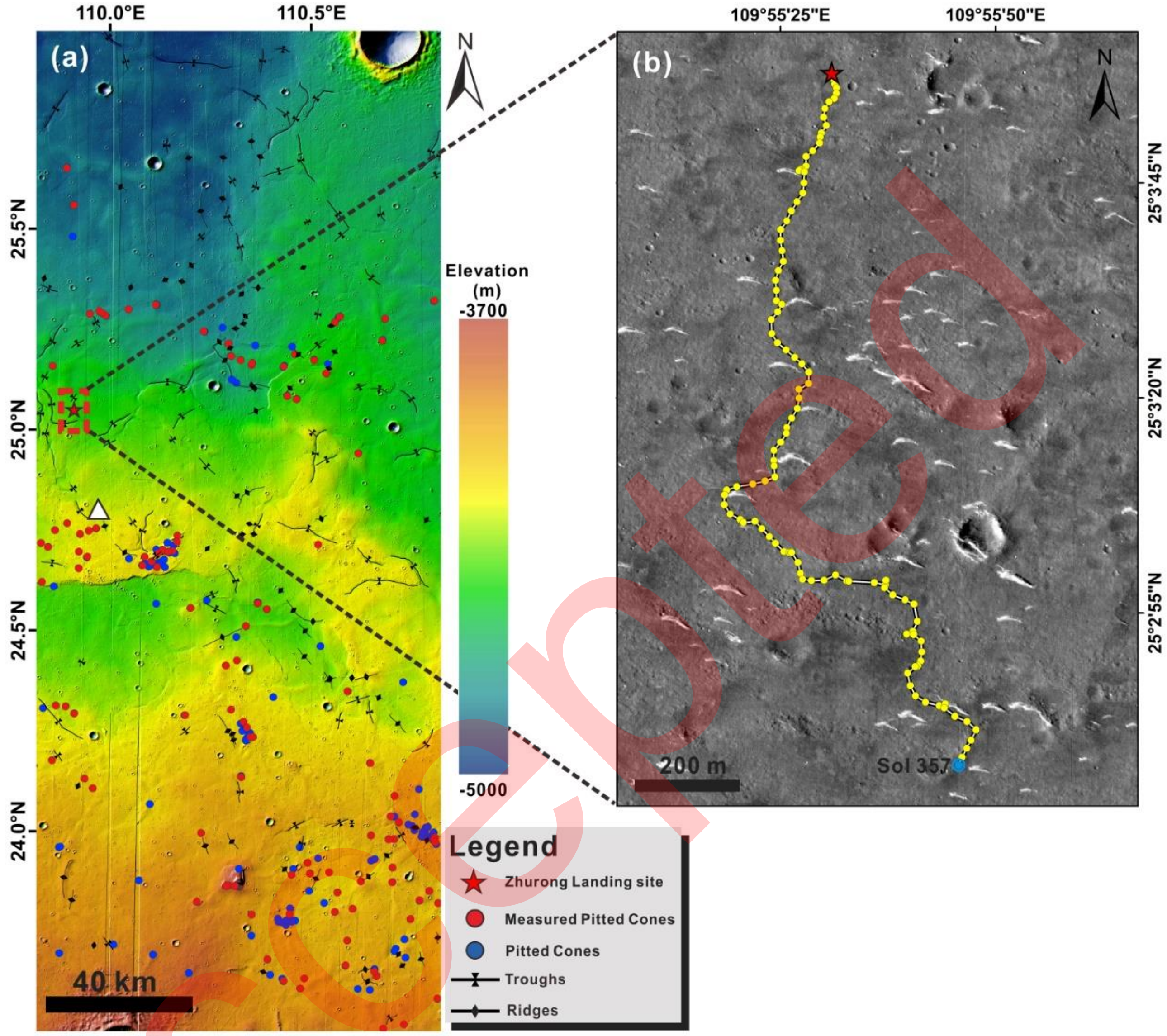

Figure 3 The distribution of pitted cones in the Zhurong landing area. (a). Identified pitted cones, troughs, and ridges in the Zhurong landing region. The white triangle indicates the nearest pitted cone from the location of the Zhurong rover at Sol 357. The red rectangle in the dashed line indicates the location of (b). The red star indicates the Zhurong rover's landing site in both (a) and (b). The color-coded map is a mosaic of DEMs on shaded relief derived from stereo pair of images of the Tianwen-1 HiRIC instrument. Note that the blue points indicate pitted cones that have elongated plan-view shapes and are strongly eroded, which are not used to make the measurement. (b). The traverse of Zhurong rover by Sol 357, and the traveled distance is about 1921 m. The background image is a mosaic of the HiRIC instrument. The yellow points indicate the places where the Zhurong rover's Navigation and Topography Camera obtained images.

4.1 Morphological Characteristics

We performed a comprehensive analysis of the pitted cones in the study region, by utilizing a combination of HiRIC and HiRISE images. Our observations revealed a variety of degrees of preservation and morphological characteristics of these cones. Some pitted cones were well preserved with distinct summit depression rims (Figure 4a), while others were degraded with small craters on the flanks and indistinct cone shapes (Figure 4b). Some cones were only partially preserved with evident impact craters on its base (Figure 4c). We also observed a few well-preserved cones with elongated plan-view shapes (Figure 4d), as well as cones that coalesced with each other and appeared as twin cones or cone clusters (Figure 4e, f). One pitted cone was connected with a ridge (Figure 4g) that has flow-like features along its southwest side (Figure 4h). The width of the ridge was around 200 m, and its height was roughly 10 m. Among all of these pitted cones we identified, one cone showed an obvious flow-like feature at its foot (Figure 4i), and the floor of its summit depression contained a high concentration of boulders (Figure 4j). This particular cone was also the closest pitted one to the Zhurong rover in the rover's traveling direction. We further noticed that apart from the cones similar to the one in Figure 4b, almost all the other pitted cones exhibited albedo variations on their flanks (Figure 4k, l). The upper part of the flank was covered with relatively darker materials, while the lower part has a relatively high albedo (Figure 4k). The albedo variations were more noticeable on the southern flank of the pitted cones.

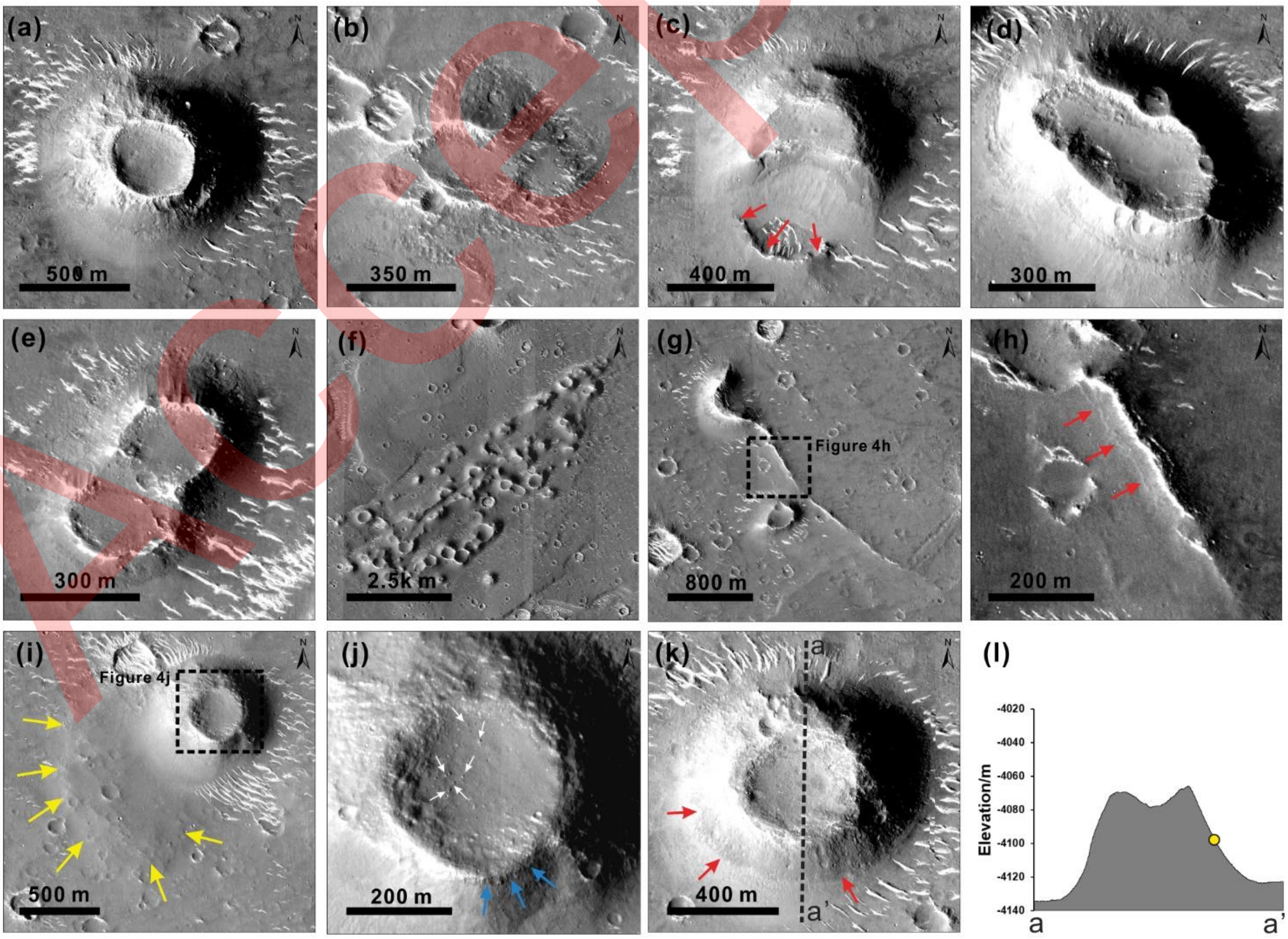

Figure 4 The detailed characteristics of pitted cones in the vicinity of the Zhurong landing site. (a) A relatively pristine pitted cone, centered at 110.045 °E, 25.299 °N. (b) A slightly eroded pitted cone, centered at 109.845 °E,

24.707 °N. (c) A severely eroded pitted cone. The red arrows indicate the rim of an impact crater. The center of the image is 109.949 °E, 25.287 °N. (d) A pitted cone with an elongated summit crater, centered at 109.988 °E, 25.284 °N. (e) Coalesced double cones, centered at 110.432 °E, 25.157 °N. (f) Cluster of pitted cones, centered at 110.124 °E, 24.691 °N. (g) A pitted cone connected with a linear ridge. The white box indicates the location of (h). The image is centered at 110.5 °E, 25.194 °N. (h) Flow-like features, indicated by red arrows, are associated with the ridge structure. (i) A pitted cone with flow-like features, whose edges are indicated by yellow arrows. The image is centered at 109.972 °E, 24.796 °N. The white box indicates the location of (j). (j) The summit crater of the pitted cone in (i) with a rough rim (the blue arrow) similar to the welded pyroclastic collar and boulders (the white arrows). (k) Relatively dark materials are identified on the upper part of some pitted cones. The red arrows indicate the boundary of the albedo variation. The image is centered at 109.856 °E, 25.158 °N. (l) The topography of the pitted cone (k). The yellow dot indicates the location of the albedo boundary marked by red arrows in (k). All images are from the HiRIC instrument (a, c, d, k: HX1_GRAS_HIRIC_DIM_0.7_0004_251515N1095850E_A; e, g, h: HX1_GRAS_HIRIC_DIM_0.7_0005_251515N1101905E_A; b, f, i, j: HX1_GRAS_HIRIC_DIM_0.7_0007_244453N1095850E_A).

4.2 Morphometric Analysis

Using the DEMs from Tianwen-1, we conducted morphometric analyses on 69 pitted cones and obtained the following results: the Wco of the cones ranges from 317 to 1363 m, with an average diameter of 758 m; the Wcr range from 93.4 to 514 m, with an average of 258.35 m; the Hco are 13–80.46 m, with an average of 36 m; and the slopes are 4–12°, with an average of 8°. The average values of Wcr/Wco, Hco/Wco, and Hco/Wcr are 0.342 (with a range of 0.22–0.48), 0.046 (with a range of 0.025–0.077), and 0.145 (with a range of 0.056–0.317), respectively. In Figure 5a, the pitted cones in our study region are mainly distributed in the middle region of the plot, while the cinder cones, rootless cones, mud volcanoes, and tuff rings/cones are mostly located in the upper left, upper right, lower left, and lower right, respectively. The cones have similar slopes to terrestrial mud volcanoes (Figure 5b), while the Wcr/Wco values fall whthin the range of terrestrial cinder cones and tuff rings/cones (Figure 5c).

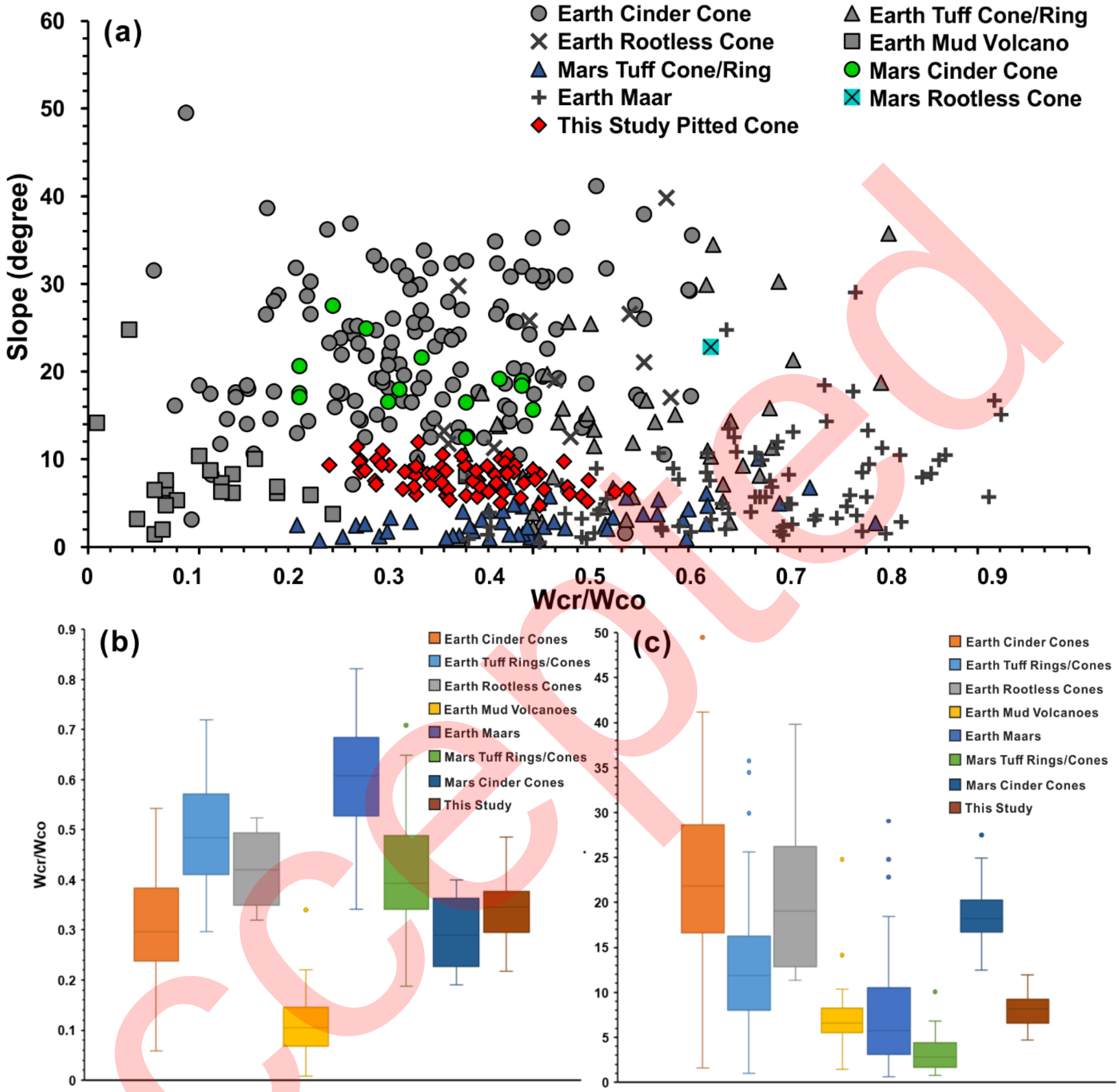

Figure 5 Plots of geometric parameters of the pitted cones on Earth and Mars. (a). Wcr/Wco vs. slope plot of pitted cones in the Zhurong landing region and martian and terrestrial cone-shaped features. The morphological parameters of the pitted cones in Zhurong landing region are in Table S1. The others are from the following sources: Earth Cinder Cones (Pike, 1978; Hasenaka and Carmichael, 1985; Carn, 2000; Rodríguez et al., 2010), Earth Mud Volcanoes (Ivanov et al., 1996; Delisle et al., 2002; Kholodov, 2002; Brož and Hauber, 2013), Earth Tuff Rings/Cones (Brož and Hauber, 2013), Earth Maar (Pike, 1978), Earth Rootless Cones (Pike, 1978); Mars Tuff Rings/Cones (Brož and Hauber, 2013), Mars Rootless Cones (Noguchi and Kurita, 2015), Mars Cinder Cones (Brož and Hauber, 2012). (b) and (c). Box plots of the slopes and Wcr/Wco of pitted cones. The red line indicates the mean values of Wcr/Wco or slope of pitted cones in the Zhurong landing area.

5. Discussion

5.1 Origin of pitted cones in the Zhurong landing region

The pitted cones investigated within the Zhurong landing area share morphological similarities with various conical landforms as mentioned in the introduction (such as pingos, dirt cones, rootless cones, scoria/cinder cones, tuff rings/cones, and mud volcanoes). These conical landforms can be classified into four main categories based on their formation mechanism: (1) ice-related cones (pingos, dirt cones), (2) phreatomagmatic cones (rootless cones), (3) monogenetic volcanoes (which include dry cones such as scoria/cinder cones and wet cones like tuff ring/cones), and (4) sedimentary cones (mud volcanoes) (Burr et al., 2009a; Silva and Lindsay, 2015). This section compares the specific morphological characteristics and formation mechanisms of the pitted cones in the Zhurong landing region with similar conical features of different origins and discusses the most probable origin of the investigated pitted cones.

5.1.1 Ice-related cones

5.1.1.1 Pingos

Pingos are small domical hills formed by the continuous supply and freezing of pressurized groundwater, and usually have an ice core (Burr et al., 2009a; Dundas and McEwen, 2010). Fully developed pingos have radial cracks on the top due to the expansion of the ice core, and a summit depression may form with the sublimation and collapse of the pingo (Burr et al., 2009a). The materials and textures of the pingos are consistent with the geological context (Dundas and McEwen, 2010). However, the investigated pitted cones have higher albedo than their surroundings (Figure 4), and even different from their base to summit (Figure 4k). Additionally, all of the pitted cones have summit pits, but no cone with radial cracks on top. Some pitted cones were partially destroyed by impact craters (Figure 4c), and if they are pingos, they should collapse due to the exposure and rapid exhaust of the ice cores. Based on these observations, it can be concluded that the observed characteristics of the pitted cones do not support an origin as pingos.

5.1.1.2 Dirt cones

Dirt cones are remnants of glaciers formed by debris that partially cover the glacier and protect the underlying ice from ablation (Swithinbank, 1950). However, the shapes of the dirt cones are seldom perfectly conical (Swithinbank, 1950), which is inconsistent with the investigated pitted cones. Isolated pitted cones in Isidis Planitia, similar to the cones in our study area, have been proposed to be dirt cones and are distributed across the whole floor of the Isidis basin (Guidat et al., 2015).

Nonetheless, the pitted cones in the Utopia Planitia are only found along the southern margin of the basin (Ye et al., 2021), suggesting that pitted cones of the two regions may not be controlled by the same process. Moreover, the pitted cones in the Zhurong landing region do not show any specific spatial pattern, unlike the large number of aligned cones in the Isidis Planitia. Therefore, the pitted cones in the Zhurong landing region are inconsistent with the origin of the pitted cones in the Isidis Planitia and the dirt cones.

5.1.2 Phreatomagmatic cones

Rootless cones, also known as pseudocraters, are formed by the deposition of ejected debris during a phreatomagmatic explosive eruption, which occurs when lava flow moves over a wet substrate (Greeley and Fagents, 2001; Fagents et al., 2002). The formation of rootless cones is dependent on the presence of two critical factors: lava flows and surface or near-surface water/ice. Although the presence of subsurface water/ice in our study area is suggested by the rampart craters (Mouginis-Mark, 1987; Ye et al., 2021; Niu et al., 2022), there is no evidence of lava flows widely distributed in the area. In fact, a recent study (Li et al., 2022) found no evidence of lava flows in the subsurface structural profile derived from the low-frequency radar data of Zhurong, but instead identified two fining-upward sedimentary layers with a combined thickness of 80 m below the regolith (Li et al., 2022). In contrast, putative rootless cone fields, such as those in Amazonis Planitia and Central Elysium Planitia, are covered by visible lava flows (Fagents et al., 2002; Noguchi and Kurita, 2015). The rootless cones in central Elysium Planitia also exhibit unique moats and concentric structures, which are not present in the investigated pitted cones. Therefore, due to the lack of widespread lava flows in the Zhurong landing region, the formation of rootless cones is an unlikely hypothesis for the origin of the investigated pitted cones.

5.1.3 Monogenetic volcanoes

5.1.3.1 Dry monogenetic volcanoes: scoria or cinder cones

The formation of cinder or scoria cones is mainly formed by the accumulation of pyroclastic materilas and volcanic ash in a dry environment, resulting in small conical landforms with bowl-shaped summit pits (Wood, 1980; Silva and Lindsay, 2015). The SP Crater in Arizona's San Francisco volcanic field, which is a typical terrestrial scoria/cinder cone, is used as a comparison to study the pitted cones in the Tharsis region of Mars (Brož and Hauber, 2012). The pitted cones in our study area have similar conical shape and near-circular summit pits, but they lack the lava flows that are usually present around terrestrial scoria/cinder cones. Although there is a pitted cone with a basal flow-like feature (Figure 4i), summit depression boulders, and rough rim (Figure 4j) similar to a welded top pyroclastic collar (Németh, 2010), it cannot be determined whether the flow-like feature is lava flow due to the lack of spectral data coverage. Additionally, this cone's slope (~10°) is smaller than that of typical cinder cone. Most of the pitted cones in the Zhurong landing region do not show evidence of flow-like features. On Earth, the repose angle of loose scoria is 33°, and the slope of well-preserved scoria/cinder cones is usually ~30° (de Silva and Lindsay, 2015). The maximum slope of the pitted cones in our study area is ~12°, with an average of 8°, which is much smaller than that of terrestrial scoria/cinder cones (Figure 5b). It should be noted that the environmental conditions between the Earth and Mars are different. Pyroclastic particles cannot reach the angle of repose as they spread further under the lower gravity and atmospheric pressure conditions of Mars (Brož et al., 2014; Brož et al., 2015), which means that the slope of cinder cones on Mars is less than 30°. Nevertheless, the average slope of Martian cinder cones (20°) is still larger than the maximum slope of the pitted cones in the Zhurong landing region. This may indicate that the investigated cones have a different composition than cinder cones. To summarize, the much lower slope and lack of flow-like features of the investigated pitted cones indicate that they have a different origin from the scoria/cinder cones.

5.1.3.2 Wet monogenetic volcanoes: tuff rings/cones

Tuff rings/cones are formed by phreatomagmatic eruptions when ascending magma interacts with groundwater (Farrand et al., 2005; Brož and Hauber, 2013; de Silva and Lindsay, 2015). The summit pit floors of the tuff rings/cones are usually lower than the preexisting surface due to the excavation of the substrate (Brož and Hauber, 2013). We did not observe similar characteristics on the topographic profiles of the investigated pitted cones. On Earth, the average Wcr/Wco of tuff rings is ~0.49 (Pike, 1978) and their slope is 2–10° (de Silva and Lindsay, 2015), while the tuff cones usually have slopes of 20–30° (de Silva and Lindsay, 2015). Brož and Hauber (2013) investigated the pitted cones in the Nephentes/Amenthes region of Utopia Planitia which is in the south of our study area. They proposed those cones to be tuff rings/cones and reported the Wcr/Wco and slopes of those cones are 0.42 and below 10° (Brož and Hauber, 2013). The pitted cones in our study region have an average Wcr/Wco of 0.34, much lower than typical tuff rings, and their slopes range from 4 to 12°, lower than those of typical tuff cones (Figure 5c). In addition, the basal diameters of the pitted cones reported by Brož and Hauber (2013) range from ~3 to 15 km, which are larger than the pitted cones (~300–1300 m) in the Zhurong landing region. Therefore, we concluded that the investigated pitted cones are inconsistent with tuff rings/cones both on Earth and Mars.

5.1.4 Sedimentary cones

A mud volcano is a kind of sedimentary landform with a conical shape, usually formed as a result of the eruption of low-density argillaceous materials (Kopf, 2002; Mazzini et al., 2007; Salvatore and Christensen, 2014). The Mars Surface Composition Detector onboard the Zhurong rover has observed hydrated sulfate/silica materials (Liu et al., 2022b; Liu et al., 2022c). These hydrated minerals are interpreted to be precipitates from the subsurface salty water in the capillary fringe zone (Liu et al., 2022b) and altered volcaniclastic soils in limited or ephemeral water (Liu et al., 2022c). The rocks with hydrated minerals are widely distributed along the traverse of Zhurong (Liu et al., 2022b), which indicates there was an extensive subsurface water-bearing layer. The aquiferous layer may be formed during rapid deposition. The subsurface sedimentary strata, detected by the penetrating radar of the Zhurong rover, also indicate that the Utopia Planitia had been filled by episodic flooding sediments (Li et al., 2022). There are also widely distributed mudflows within the Utopia Planitia about 130 km to the north of the Zhurong landing region (Ivanov et al., 2014; Cuřín et al., 2022). Cuřín et al. (2022) proposed that there has been a large volume of mud reservoir in the Utopia Planitia, which may provide sufficient source materials for the mud volcanoes. All of these previous studies support a mud volcano origin for the pitted cones in the Zhurong landing region.

On Earth, mud volcanoes are divided into three categories according to their eruption intensity: (1) Lokbatan type, which has strong explosive eruption and short activity time. (2) Chikishlyar type, which has a quiet eruption, weak eruption activity, and long duration. (3) Schugin type, which is a transitional type that has intermittent explosive eruptions during longer phases of continuous calm eruptions (Dimitrov, 2002). The Wcr/Wco ratio is an indicator of the magnitude of the explosive activity (Wood, 1980; Fagents et al., 2002; Noguchi and Kurita, 2015), which means that a higher value suggests a more intensive eruption. Mud volcanoes in Azerbaijan on the Earth have an average Wcr/Wco of 0.13 (Brož and Hauber, 2013), lower than the value (0.34) of the pitted cones in the Zhurong landing site (Figure 5c). Therefore, the pitted cones in the Zhurong landing area could have erupted more violently than Azerbaijan mud volcanoes. Komatsu et al. (2016) observed flat mud pies with gentle slopes and mud flows with levees in Chryse Planitia. These features are usually composed of mud with higher porosity or lower cohesion (Kopf, 2002; Burr et al., 2009b), which means the mud has a low viscosity. We did not find mud pies or flows in the Zhurong landing region, which may indicate that the mud has a higher viscosity. Low-viscosity mud under extreme Martian surface conditions exhibits similar fluid properties to lava flows on Earth (Brož et al., 2020). Thus, the high viscosity of mud may result in explosive eruptions similar to explosive magmatic volcanism.

There usually are fields of boulders with scales of several meters around the explosive mud volcanoes (Burr et al., 2009b), but these boulders may be buried by the dust in our study area.

Based on the above evidence, we propose that the pitted cones in the Zhurong landing region are explosive mud volcanoes. During an explosive eruption, there will be more mud breccia ejected into the atmosphere and desiccated due to the instability of liquid water, which leads to the missing of associated mudflows (Brož et al., 2019), consistent with what we observed in the study region.

5.2 A Scenario for Pitted Cone Formation

Mud volcanism is a surface manifestation of geological processes in the deep subsurface sedimentary succession (Dimitrov, 2002; Kopf, 2002). Based on the explosive mud volcano origin suggested by the discussion above, we propose a hypothetical scenario on the subsurface geological evolution of the study region (Figure 6).

The formation of explosive mud volcanoes needs sufficient subsurface under-compacted sediments reaching overpressure and some trigger events (Dimitrov, 2002). We propose four stages for the generation of explosive mud volcanoes (Figure 6). The first stage is the formation of under-compacted sediments (Figure 6a). The northern lowlands of Mars are covered by the Vastitas Borealis Formation (VBF) (Tanaka et al., 2014). The VBF, several hundred meters of fine-grained materials, may be the remnant sediments of a Hesperian Ocean (Kreslavsky and Head, 2002; Carr and Head, 2003) fed by the outflow channels formed by the catastrophic circum-Tharsis floods (Carr and Head, 2003). The outflow channels episodically transported significant quantities of sediments into the northern lowlands from the southern highlands (Fairén et al., 2003). During these periods, the rapid sedimentations could produce a large amount of under-compacted sediments to support the formation of explosive mud volcanoes. The second stage is the generation of overpressurized sediments and diapiric structures (Figure 6b). All of the sedimentary layers would rapidly freeze under atmospheric conditions similar to those of today throughout ~10000 years (Kreslavsky and Head, 2002) to form permafrost. There may be a small number of fluid materials at the bottom of the permafrost due to the compaction of overburden, but it is not enough to overcome the lithostatic pressure. Although impact craters could result in the melting of permafrost and the eruption of fluid sediments, there is no correlation between pitted cones and craters in their distribution. Hence, an anomalously high heat flow would be required to promote the melting of subsurface ice and the generation of overpressurized sediments. These overpressurized sediments then intruded into the upper layers to form diapirs. We observed some ridges similar to dikes found in eastern Utopia Planitia (Pedersen et al., 2010), and they are connected to the pitted cones (Figure 4g, h), which

https://engine.scichina.com/doi/10.1007/s11430-022-1119-1

could provide evidence of the magmatic activities during the formation of the pitted cones. The third stage is explosive eruption (Figure 6c). Massive materials, composed of mud breccia, ice, and surrounding rocks, would explosively erupt to the surface when the interior pressure of fluid sediments exceeded the overburden. The explosive eruption may account for a mass of volatiles (such as methane and vapors) released from the frozen sediments or the evaporation of water. But it is also an open question whether there are still gases released from the pitted cones. The fourth stage is the formation of the pitted cone (Figure 6d). The mud and ice-cemented ejecta composed a mud volcano which is the present pitted cone. Although the ground-penetrating radar of Zhurong did not find liquid water or ice (Li et al., 2022), it is not sure whether the permafrost and fluid sediments that fed the mud volcanoes still exist in a deeper subsurface.

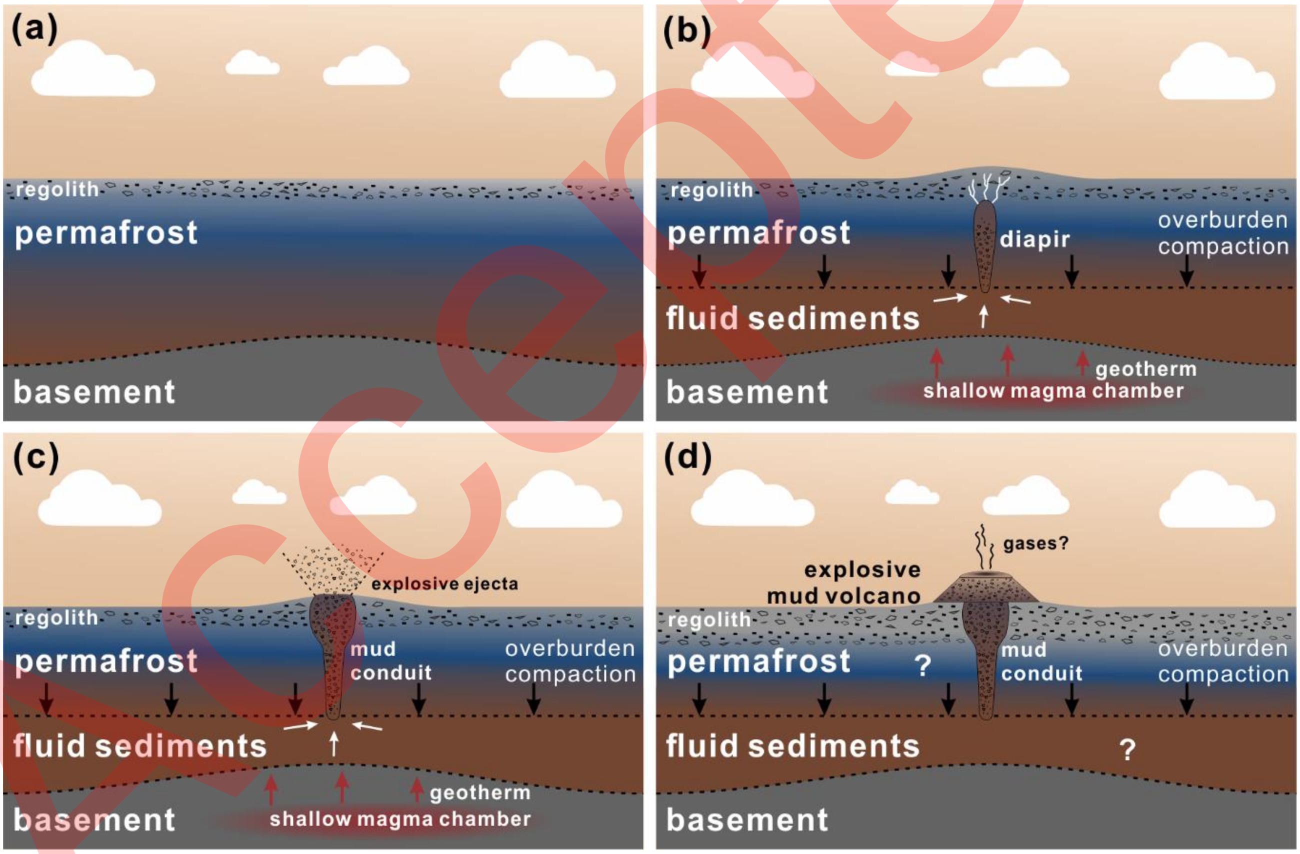

Figure 6 Sketch map of the generating stages of explosive mud volcanoes. (a). The VBF, remnants of the Hesperian Ocean, was frozen at its upper part and still fluid at its lower part, which provided under-compacted sediments. (b). Fluid sediments became overpressurized and intruded into the overburden due to the top compaction and anomalous high geotherm. Resulting in the formation of a diapiric structure. The white arrows indicate the flow direction of mud. The dash straight line indicates possible boundary between the permafrost and fluid sediments. (c). The explosive eruption ejected massive materials which are composed of mud breccia, surrounding rocks, ice, and gasses. The white arrows indicate the flow direction of mud. (d). The mud and ice cemented ejecta and generated a pitted cone. The features are not to scale.

https://engine.scichina.com/doi/10.1007/s11430-022-1119-1

5.3 Key In-situ Observations from the Zhurong Rover

In this study, we mainly used topographic and geomorphologic data to study the pitted cones. To further confirm the origin of the pitted cones, in-situ exploration of the Zhurong rover will be critical. At present, the rover has been heading south, and the nearest pitted cone is about 14.5 km from its location at Sol 357 (Figure 3b). There are various scientific payloads aboard the Zhurong rover, including Mars Surface Composition Detector (MarSCoDe), Navigation and Terrain Camera (NaTeCam) and Mars Rover Penetrating Radar (RoPeR) (Zou et al., 2021). The MarSCoDe instrument is composed of a laser-induced breakdown spectroscopy (LIBS) spectrometer and a passive spectrometer. The spectral range of LIBS is 240–850 nm, and the spectral resolutions are 0.1 nm (240–340 nm), 0.2 nm (340–540 nm), and 0.3 nm (540–850 nm). The passive spectrometer can acquire spectra ranging from 850 to 2400 nm and has a spectral resolution of 3–12 nm (Zou et al., 2021; Xu et al., 2021). It can obtain information on the elemental and mineral composition of the Martian surface. NaTeCam can obtain color images and high-resolution terrain construction of patrolling areas (Liang et al., 2021). The RoPeR instrument can detect the martian subsurface structure up to 100 m deep (Zhou et al., 2020; Zou et al., 2021).

The MarSCoDe instrument can distinguish the igneous or sedimentary origin of the pitted cones. Cones with an igneous origin include cinder (scoria) cones, tuff rings/cones, maars, and rootless cones. They are all related to the magmatic or phreatomagmatic eruption/emplacement and are mainly composed of basaltic pyroclastic materials (Wood, 1979; Valentine and Gregg, 2008). Cones with a sedimentary origin are mainly mud volcanoes and they are usually composed of low-density sedimentary materials such as under-compacted evaporites and clays with corresponding minerals including gypsum, halite, kaolinite, smectite, and vermiculite groups (Kopf, 2002).

The RoPeR instrument can detect subsurface geological structures and constrain the thickness of regolith, rock, and ice layers (Tan et al., 2021; Zou et al., 2021). The RoPeR has two channels, including a low-frequency channel (15–95 MHz) and a high-frequency channel (450–2150 MHz) (Zhou et al., 2020). The channels can penetrate to depths of 10–100 m (resolution of a few meters) and 3–10 m (resolution of a few centimeters) respectively (Zhou et al., 2020). The horizontal space of the RoPeR traces is up to 50 cm (Li et al., 2022). Based on the radar data of the Zhurong rover, Li et al. (2022) observed layered subsurface sediments. According to the basic parameters of RoPeR and the recent research on the subsurface structure of the Zhurong landing region, we list possible observations of the instrument in distinguishing the origins of the pitted cones:

(1) Pingos. To clearly identify the pingos, the direct evidence is ice core (Dundas and McEwen, 2010). The low-frequency penetrating radar (<80 MHz) can detect the ice structure of pingos

(Yoshikawa et al., 2006). The dielectric constant ranges from 3 to 4 for the massive ice core of pingos on Earth, but the value can be reduced by air bubbles with high density (Yoshikawa et al., 2006). There will be a distinct boundary between the ice core and the surrounding silty permafrost or bedrock (Yoshikawa et al., 2006). Due to the melting or sublimation of the ice core, pingos would be collapsed into pingo scar, which is difficult to be identified through penetrating radar.

(2) Rootless cones. The subsurface lava flows should be detected. There is no root on the radar profile, because rootless cones are developed on the lava flows (Fagents et al., 2002).

(3) Effusively erupted mud volcanoes. Complex subsurface geological structures with large numbers of fractures, faults, or folds generated by regional tectonic activities are the targets of exploration (Dimitrov, 2002). In addition, density inversion will form a typical diapir structure (Kopf, 2002; Mazzini and Etiope, 2017) and when multiple stages of mud eruption happen, a "Christmas tree" structure can be formed in the subsurface (Praeg et al., 2009; Mascle et al., 2014; Mazzini and Etiope, 2017). On Earth, this "Christmas tree" structure is usually developed on the seafloor and exhibits interbedding of mud volcanic ejecta and seafloor sediments. The special subsurface structure with a common scale of more than 1 km wide and extending to several hundred milliseconds deep from the surface indicates a buried mud volcano (Mascle et al., 2014; Mazzini and Etiope, 2017).

(4) Explosive mud volcanoes. Intrusive structures such as igneous dikes or sills should be detected. These dikes or sills can be surrounded by fine-grained sedimentary materials that may contain ice or water. In the Zhurong landing region, the ridges (Figure 4g, h) similar to dikes have an average width of 150 m. RoPeR can distinguish the dikes from the surrounding sedimentary rocks.

6. Conclusion

The morphological characteristics of pitted cones in the Zhurong landing region indicate an explosive mud volcano origin. These cones were formed by the explosive eruption of overpressurized sediments derived from the frozen outflow channel materials under the heating of a shallow magmatic chamber and compaction of overburden. The explosive mud volcano origin of the investigated pitted cones supports the hypothesis of the ancient ocean in the northern lowlands. It also suggests a habitable subsurface environment with suitable temperature and liquid water, which is beneficial to the generation of life. We proposed some scientific targets according to the payloads of Zhurong to verify the explosive mud volcano origin of the investigated pitted cones. The potential deep source materials of the habitable subsurface environment transported by mud volcanoes are important for future in-situ explorations and sample return missions of Mars.

Acknowledgments

The Tianwen-1 data used in this study are available at https://moon.bao.ac.cn/web/enmanager/zygj and provided by China National Space Agency and the Science and Application Center for Moon and Deep Space Exploration. We appreciate the editorial handling by Editor Dr. Yamin Li. The reviews by Prof. Ernst Hauber and an anonymous reviewer greatly improved the manuscript. The authors thank Prof. Qiliang Sun in the College of Marine Science and Technology, China University of Geosciences for the discussion on mud volcanoes. This study was supported by the Strategic Priority Research Program of the Chinese Academy of Sciences (XDB 41000000), the National Natural Science Foundation of China (42273041, 42272274, 41830214), and the Pre-research Project on Civil Aerospace Technologies of CNSA (D020101).

References

Brož P, Hauber E. 2012. A unique volcanic field in Tharsis, Mars: Pyroclastic cones as evidence for explosive eruptions. Icarus 218, 88-99.

Brož P, Hauber E. 2013. Hydrovolcanic tuff rings and cones as indicators for phreatomagmatic explosive eruptions on Mars. Journal of Geophysical Research: Planet, 118, 1656-1675.

Brož P, Čadek O, Hauber E, Rossi A P J E, Letters P S. 2014. Shape of scoria cones on Mars: Insights from numerical modeling of ballistic pathways. Earth and Planetary Science Letters, 406, 14-23.

Brož P, Čadek O, Hauber E, Angelo Pio Rossi A P. (2015). Scoria cones on Mars: Detailed investigation of morphometry based on high‐resolution digital elevation models. Journal of Geophysical Research: Planet, 120(9), 1512-1527.

Brož P, Hauber E, Van de Burgt I., Špillar V., Michael G. 2019. Subsurface sediment mobilization in the southern Chryse Planitia on Mars. Journal of Geophysical Research: Planet, 124, 703-720.

Brož P, Hauber E, Wray J J, Michael G. 2017. Amazonian volcanism inside Valles Marineris on Mars. Earth and Planetary Science Letters, 473, 122-130.

Brož P, Krýza O, Wilson L, Conway S J, Hauber E., Mazzini A., Raack J, Balme M R, Sylvest M E, Patel M R. 2020. Experimental evidence for lava-like mud flows under Martian surface conditions. Nature Geoscience, 13, 403-407.

Burr D M, Tanaka K L, Yoshikawa K. 2009a. Pingos on Earth and Mars. Planetary and Space Science, 57, 541-555.

Burr D M, Bruno B C, Lanagan P D, Glaze L S, Jaeger W L, Soare R J, Tseung J -M W B, Skinner Jr J A, Baloga S M. 2009b. Mesoscale raised rim depressions (MRRDs) on Earth: A review of the characteristics, processes, and spatial distributions of analogs for Mars. Planetary and Space Science, 57, 579-596.

Carn S A. 2000. The Lamongan volcanic field, East Java, Indonesia: physical volcanology, historic activity and hazards. Journal of Volcanology and Geothermal Research 95, 81-108.

Carr M H, Head J W. 2003. Oceans on Mars: An assessment of the observational evidence and possible fate. Journal of Geophysical Research: Planets 108.

Clifford S M, Parker T J. (2001). The evolution of the Martian hydrosphere: Implications for the fate of a primordial ocean and the current state of the northern plains. Icarus, 154(1), 40-79.

Cuřín V, Brož P, Hauber E, Markonis Y. 2022. Mud flows in Southwestern Utopia Planitia, Mars. Icarus, 389, 115266.

Dapremont A M, Wray J J. 2021. Igneous or Mud Volcanism on Mars? The Case Study of Hephaestus Fossae. Journal of Geophysical Research: Planets 126, e2020JE006390.

de Pablo M Á., Komatsu G. 2009. Possible pingo fields in the Utopia basin, Mars: Geological and climatical implications. Icarus 199, 49-74.

de Silva S, Lindsay J M. 2015. Primary volcanic landforms, The encyclopedia of volcanoes. Elsevier, 273-297.

Delisle G, Von Rad U, Andruleit H, Von Daniels C, Tabrez A, Inam A. 2002. Active mud volcanoes on-and offshore eastern Makran, Pakistan. International Journal of Earth Sciences 91, 93-110.

Dimitrov L I. 2002. Mud volcanoes—the most important pathway for degassing deeply buried sediments. Earth-Science Reviews 59, 49-76.

Dundas C M, McEwen A S. 2010. An assessment of evidence for pingos on Mars using HiRISE. Icarus 205, 244-258.

Fagents S, Lanagan P, Greeley R. 2002. Rootless cones on Mars: A consequence of lava-ground ice interaction. Geological Society, London, Special Publications 202, 295-317.

Fairén A G, Dohm J M, Baker V R, de Pablo M A, Ruiz J, Ferris J C. Anderson, R.C., 2003. Episodic flood inundations of the northern plains of Mars. Icarus 165, 53-67.

Farrand W H, Gaddis L R, Keszthelyi L. 2005. Pitted cones and domes on Mars: Observations in Acidalia Planitia and Cydonia Mensae using MOC, THEMIS, and TES data. Journal of Geophysical Research: Planets 110.

Frey H, Jarosewich M. 1982. Subkilometer Martian volcanoes: Properties and possible terrestrial analogs. J Geophys Res, 87, 9867-9879.

Greeley R, Fagents S A. 2001. Icelandic pseudocraters as analogs to some volcanic cones on Mars. Journal of Geophysical Research: Planets 106, 20527-20546.

Guidat T, Pochat S, Bourgeois O, Souček O. 2015. Landform assemblage in Isidis Planitia, Mars: Evidence for a 3 Ga old polythermal ice sheet. Earth and Planetary Science Letters 411, 253-267.

Hasenaka T, Carmichael I S. 1985. The cinder cones of Michoacán—Guanajuato, central Mexico: their age, volume and distribution, and magma discharge rate. Journal of Volcanology and Geothermal Research 25, 105-124.

Hemmi R, Miyamoto H. 2017. Distribution, morphology, and morphometry of circular mounds in the elongated basin of northern Terra Sirenum, Mars. Progress in Earth and Planetary Science 4, 1-15.

Hodges C A, Moore H J. 1994. Atlas of volcanic landforms on Mars. US Government Printing Office.

Huang H, Liu J, Wang X, Chen Y, Zhang Q, Liu D, Yan W, Ren X. (2022). The Analysis of Cones within the Tianwen-1 Landing Area. Remote Sensing, 14(11), 2590.

Ivanov M, Limonov A, Van Weering T C. 1996. Comparative characteristics of the Black Sea and Mediterranean Ridge mud volcanoes. Marine geology 132, 253-271.

Ivanov M A, Head J W. (2001). Chryse Planitia, Mars: Topographic configuration, outflow channel continuity and sequence, and tests for hypothesized ancient bodies of water using Mars Orbiter Laser Altimeter (MOLA) data. Journal of Geophysical Research: Planets, 106(E2), 3275-3295.

Ivanov M A, Hiesinger H, Erkeling G, Reiss D. 2014. Mud volcanism and morphology of impact craters in Utopia Planitia on Mars: Evidence for the ancient ocean. Icarus, 228, 121-140.

Kargel J S, Baker V R, Begét J E, Lockwood J F, Péwé T L, Shaw J S, Strom R G. 1995. Evidence of ancient continental glaciation in the Martian northern plains. Journal of Geophysical Research: Planets 100, 5351-5368.

Keszthelyi L, Jaeger W, Dundas C, Martínez-Alonso S, McEwen A, Milazzo M. 2010. Hydrovolcanic features on Mars: Preliminary observations from the first Mars year of HiRISE imaging. Icarus 205, 211-229.

Kholodov V. 2002. Mud volcanoes, their distribution regularities and genesis: communication 1. Mud volcanic provinces and morphology of mud volcanoes. Lithology and Mineral Resources 37, 197-209.

Komatsu G, Okubo C H, Wray J J, Ojha L, Cardinale M, Murana A, Orosei R, Chan M A, Ormö J, Gallagher R. 2016. Small edifice features in Chryse Planitia, Mars: assessment of a mud volcano hypothesis. Icarus 268, 56-75.

Kopf A J. 2002. Significance of mud volcanism. Reviews of geophysics 40, 2-1-2-52.

Kreslavsky M A, Head J W. 2002. Fate of outflow channel effluents in the northern lowlands of Mars: The Vastitas Borealis Formation as a sublimation residue from frozen ponded bodies of water. Journal of Geophysical Research: Planets 107, 4-1-4-25.

Lanz J K, Saric M B. 2009. Cone fields in SW Elysium Planitia: hydrothermal venting on Mars? Journal of Geophysical Research: Planets 114.

Lanz J K, Wagner R, Wolf U, Kröchert J, Neukum G. 2010. Rift zone volcanism and associated cinder cone field in Utopia Planitia, Mars. Journal of Geophysical Research: Planets 115 (E12).

Li C, Zheng Y, Wang X, Zhang J, Wang Y, Chen L, Zhang L, Zhao P, Liu Y, Lv W, Liu Y, Zhao X, Hao J, Sun W, Liu X, Jia B, Li J, Lan H, Fa W, Pan Y, Wu F. 2022. Layered subsurface in Utopia Basin of Mars revealed by Zhurong rover radar. Nature, 610, 308-312.

Liang X, Chen W, Cao Z, Wu F, Lyu W, Song Y, Li D, Yu C, Zhang L, Wang L. (2021). The navigation and terrain cameras on the Tianwen-1 Mars rover. Space Science Reviews, 217, 1-20.

Liu J, Li C, Zhang R, Rao W, Cui X, Geng Y, Jia Y, Huang H, Ren X, Yan W. 2022a. Geomorphic contexts and science focus of the Zhurong landing site on Mars. Nature Astronomy, 6, 65-71.

Liu Y, Wu X, Zhao Y Y S, Pan L, Wang C, Liu J, Zhao Z, Zhou X, Zhang C, Wu Y, Wan W, Zou Y. 2022b. Zhurong reveals recent aqueous activities in Utopia Planitia, Mars. Science advances, 8(19), eabn8555.

Liu C, Ling Z, Wu Z, Zhang J, Chen J, Fu X, Qiao L, Liu P, Li B, Zhang L, Xin Y, Shi E, Cao H, Tian S, Wan S, Bai H, Liu J. 2022c. Aqueous alteration of the Vastitas Borealis Formation at the Tianwen-1 landing site. Communications Earth & Environment, 3, 1-11.

Malin M C, Bell J F, Cantor B A, Caplinger M A, Calvin W M, Clancy R T, Edgett K S, Edwards L, Haberle R M, James P B. 2007. Context camera investigation on board the Mars Reconnaissance Orbiter. Journal of Geophysical Research: Planets 112.

Mascle J, Mary F, Praeg D, Brosolo L, Camera L, Ceramicola S, Dupré S. 2014. Distribution and geological control of mud volcanoes and other fluid/free gas seepage features in the Mediterranean Sea and nearby Gulf of Cadiz. Geo-Marine Letters 34, 89-110.

Mazzini A, Etiope G. 2017. Mud volcanism: An updated review. Earth-Science Reviews 168, 81-112.

Mazzini A, Svensen H, Akhmanov G, Aloisi G, Planke S, Malthe-Sørenssen A, Istadi B. 2007. Triggering and dynamic evolution of the LUSI mud volcano, Indonesia. Earth and Planetary Science Letters 261, 375-388.

McEwen A S, Eliason E M, Bergstrom J W, Bridges N T, Hansen C J, Delamere W A, Grant J A, Gulick V C, Herkenhoff K E, Keszthelyi L. 2007. Mars reconnaissance orbiter's high resolution imaging science experiment (HiRISE). Journal of Geophysical Research: Planets 112.

Meng Q, Wang D, Wang X, Li W, Yang X, Yan D, Li Y, Cao Z, Ji Q, Sun T. 2021. High resolution imaging camera (HiRIC) on China's first Mars exploration Tianwen-1 Mission. Space Science Reviews 217, 1-29.

Mouginis-Mark P J. 1987. Water or ice in the Martian regolith?: Clues from rampart craters seen at very high resolution. Icarus 71, 268-286.

Mouginot J, Pommerol A, Beck P, Kofman W, Clifford S M. (2012). Dielectric map of the Martian northern hemisphere and the nature of plain filling materials. Geophysical research letters, 39(2).

Noguchi R, Kurita K. 2015. Unique characteristics of cones in Central Elysium Planitia, Mars. Planetary and Space Science 111, 44-54.

Németh K. 2010. Monogenetic volcanic fields: Origin, sedimentary record, and relationship with polygenetic volcanism, What Is a Volcano? GSA Special Paper 470, 43-65.

Oehler D Z, Allen C C. 2010. Evidence for pervasive mud volcanism in Acidalia Planitia, Mars. Icarus 208, 636-657.

Orgel C, Hauber E, van Gasselt S, Reiss D, Johnsson A, Ramsdale J D, Smith I, Swirad Z M, Séjourné A, Wilson J T, Balme M R, Conway S J, Costard F, Eke V R, Gallagher C, Kereszturi Ákos, Łosiak A, Massey R J, Platz T, Skinner J A, Teodoro L F A. (2019). Grid mapping the northern plains of Mars: A new overview of recent water‐ and ice‐related landforms in Acidalia Planitia. Journal of Geophysical Research: Planets, 124(2), 454-482.

Parker T J, Saunders R S, Schneeberger D M. (1989). Transitional morphology in west Deuteronilus Mensae, Mars: Implications for modification of the lowland/upland boundary. Icarus, 82(1), 111-145.

Parker T J, Gorsline D S, Saunders R S, Pieri D C, Schneeberger D M. (1993). Coastal geomorphology of the Martian northern plains. Journal of Geophysical Research: Planets, 98(E6), 11061-11078.

Pedersen G B M, Head J, Wilson L. 2010. Formation, erosion and exposure of Early Amazonian dikes, dike swarms and possible subglacial eruptions in the Elysium Rise/Utopia Basin Region, Mars. Earth and Planetary Science Letters 294, 424-439.

Pike R J. 1978. Volcanoes on the inner planets-Some preliminary comparisons of gross topography, Lunar and Planetary Science Conference Proceedings, 3239-3273.

Praeg D, Ceramicola S, Barbieri R, Unnithan V, Wardell N. 2009. Tectonically-driven mud volcanism since the late Pliocene on the Calabrian accretionary prism, central Mediterranean Sea. Marine and Petroleum Geology 26, 1849-1865.

Rodríguez S, Morales-Barrera W, Layer P, González-Mercado E. 2010. A quaternary monogenetic volcanic field in the Xalapa region, eastern Trans-Mexican volcanic belt: geology, distribution and morphology of the volcanic vents. Journal of Volcanology and Geothermal Research 197, 149-166.

Salvatore M, Christensen P. 2014. On the origin of the Vastitas Borealis formation in Chryse and Acidalia Planitiae, Mars. Journal of Geophysical Research: Planets 119, 2437-2456.

Skinner Jr J A, Tanaka K L. 2007. Evidence for and implications of sedimentary diapirism and mud volcanism in the southern Utopia highland–lowland boundary plain, Mars. Icarus 186, 41-59.

Smith D E, Zuber M T, Frey H V, Garvin J B, Head J W, Muhleman D O, Pettengill G H, Phillips R J, Solomon S C, Zwally H J. 2001. Mars Orbiter Laser Altimeter: Experiment summary after the first year of global mapping of Mars. Journal of Geophysical Research: Planets 106, 23689-23722.

Swithinbank C. 1950. The origin of dirt cones on glaciers. Journal of Glaciology 1, 461-465.

Tan X, Liu J, Zhang X, Yan W, Chen W, Ren X, Zuo W, Li C. 2021. Design and validation of the scientific data products for China's Tianwen-1 mission. Space Science Reviews 217, 1-22.

Tanaka K L, Skinner Jr J A, Hare T M, Joyal T, Wenker A. (2003). Resurfacing history of the northern plains of Mars based on geologic mapping of Mars Global Surveyor data. Journal of Geophysical Research: Planets, 108(E4).

Tanaka K L, Skinner Jr J A, Dohm J M, Irwin R P, Kolb E J, Fortezzo C M, Platz T, Michael G G, Hare T M. 2014. Geologic map of Mars.

Valentine G, Gregg T. 2008. Continental basaltic volcanoes—processes and problems. Journal of Volcanology and Geothermal Research 177, 857-873.

Wood C A. 1979. Monogenetic volcanoes of the terrestrial planets, Lunar and Planetary Science Conference Proceedings, 2815-2840.

Wood C A. 1980. Morphometric evolution of cinder cones. Journal of Volcanology and Geothermal Research 7, 387-413.

Wu B, Dong J, Wang Y, Li Z, Chen Z, Liu W C, Zhu J, Chen L, Li Y, Rao W. 2021. Characterization of the

Candidate Landing Region for Tianwen‐1–China's First Mission to Mars. Earth and Space Science, e2021EA001670.

Wu X, Liu Y, Zhang C, Wu Y, Zhang F, Du J, Liu Z, Xing Y, Xu R, He Z. 2021. Geological characteristics of China's Tianwen-1 landing site at Utopia Planitia, Mars. Icarus 370, 114657.

Xiao L, Wang C. 2009. Geologic features of Wudalianchi volcanic field, northeastern China: implications for Martian volcanology. Planetary and Space Science 57, 685-698.

Xu W, Liu X, Yan Z, Li L, Zhang Z, Kuang Y, Jian H, Yu H, Yang F, Liu C, Wang T, Li C, Jin Y, Shen J, Wang B, Wan W, Chen J, Ni S, Ruan Y, Xu R, Zhang C, Yuan Z, Wan X, Yang Y, Li Z, Shen Y, Liu D, Wang B, Yuan R, Bao T, Shu R. (2021). The MarSCoDe instrument suite on the Mars Rover of China's Tianwen-1 mission. Space Science Reviews, 217, 1-58.

Yan W, Liu J, Ren X, Li C, Fu Q, Wang D, Dong J, Zhang X, Chen W, Tan X. 2021. Detection Capability Verification and Performance Test for the High Resolution Imaging Camera of China's Tianwen-1 Mission. Space Science Reviews 217, 1-21.

Yan W, Ren X, Liu J, Zhang L, Chen W, Wang D, Fu Q, Tan X, Zhang X, Ai H, Wang B, Zhi Q, Huang Z, Song C. 2022. Topographic Reconstruction of the "Tianwen-1" Landing Area on the Mars Using High Resolution Imaging Camera Images. IEEE Transactions on Geoscience and Remote Sensing, 60, 1-14.

Ye B, Qian Y, Xiao L, Michalski J R, Li Y, Wu B, Qiao L. 2021. Geomorphologic exploration targets at the Zhurong landing site in the southern Utopia Planitia of Mars. Earth and Planetary Science Letters 576, 117199.

Yoshikawa K, Leuschen C, Ikeda A, Harada K, Gogineni P, Hoekstra P, Hinzman L, Sawada Y, Matsuoka N. 2006. Comparison of geophysical investigations for detection of massive ground ice (pingo ice). Journal of Geophysical Research, 111, E06S19.

Zhao J, Xiao Z, Huang J, Head J W, Wang J, Shi Y, Wu B, Wang L. 2021. Geological Characteristics and Targets of High Scientific Interest in the Zhurong Landing Region on Mars. Geophys Res Lett, e2021GL094903.

Zhou B, Shen S, Lu W, Liu Q, Tang C, Li S, Fang G. 2020. The Mars rover subsurface penetrating radar onboard China's Mars 2020 mission. Earth and Planetary Physics, 4, 345-354.

Zou Y, Zhu Y, Bai Y, Wang L, Jia Y, Shen W, Fan Y, Liu Y, Wang C, Zhang A. 2021. Scientific objectives and payloads of Tianwen-1, China's first Mars exploration mission. Advances in Space Research 67, 812-823.

https://engine.scichina.com/doi/10.1007/s11430-022-1119-1